

Transition to chaos in lid-driven square cavity flow

Tao Wang(王涛) and Tiegang Liu(刘铁钢)
Citation: Chin. Phys. B, 2021, 30 (**12**): 120508. DOI: 10.1088/1674-1056/ac3226
Journal homepage: http://cpb.iphy.ac.cn; http://iopscience.iop.org/cpb

What follows is a list of articles you may be interested in

Cascade discrete memristive maps for enhancing chaos

Fang Yuan(袁方), Cheng-Jun Bai(柏承君), and Yu-Xia Li(李玉霞)
Chin. Phys. B, 2021, 30 (**12**): 120514. DOI: 10.1088/1674-1056/ac20c7

Physical generation of random numbers using an asymmetrical Boolean network

Hai-Fang Liu(刘海芳), Yun-Cai Wang(王云才), Lu-Xiao Sang(桑鲁骁), and Jian-Guo Zhang(张建国)
Chin. Phys. B, 2021, 30 (**11**): 110503. DOI: 10.1088/1674-1056/abf4fc

Acoustic wireless communication based on parameter modulation and complex Lorenz chaotic systems with complex parameters and parametric attractors

Fang-Fang Zhang(张芳芳), Rui Gao(高瑞), and Jian Liu(刘坚)
Chin. Phys. B, 2021, 30 (**8**): 080503. DOI: 10.1088/1674-1056/ac0905

Control of chaos in Frenkel-Kontorova model using reinforcement learning

You-Ming Lei(雷佑铭) and Yan-Yan Han(韩彦彦)
Chin. Phys. B, 2021, 30 (**5**): 050503. DOI: 10.1088/1674-1056/abd74f

A multi-directional controllable multi-scroll conservative chaos generator: Modelling, analysis, and FPGA implementation

En-Zeng Dong(董恩增), Rong-Hao Li(李荣昊), and Sheng-Zhi Du(杜升之)
Chin. Phys. B, 2021, 30 (**2**): 020505. DOI: 10.1088/1674-1056/abc239

Transition to chaos in lid–driven square cavity flow*

Tao Wang(王涛)[1] and Tiegang Liu(刘铁钢)[2,†]

[1] School of Mathematics and Information Science, North Minzu University, Yinchuan 750021, China
[2] LMIB and School of Mathematical Sciences, Beihang University, Beijing 100191, China

(Received 26 August 2021; revised manuscript received 8 October 2021; accepted manuscript online 22 October 2021)

To date, there are very few studies on the transition beyond second Hopf bifurcation in a lid–driven square cavity, due to the difficulties in theoretical analysis and numerical simulations. In this paper, we study the characteristics of the third Hopf bifurcation in a driven square cavity by applying a consistent fourth-order compact finite difference scheme rectently developed by us. We numerically identify the critical Reynolds number of the third Hopf bifurcation located in the interval of $(13944.7021, 13946.5333)$ by the method of bisection. Through Fourier analysis, it is discovered that the flow becomes chaotic with a characteristic of period-doubling bifurcation when the Reynolds number is beyond the third bifurcation critical interval. Nonlinear time series analysis further ascertains the flow chaotic behaviors via the phase diagram, Kolmogorov entropy and maximal Lyapunov exponent. The phase diagram changes interestingly from a closed curve with self-intersection to an unclosed curve and the attractor eventually becomes strange when the flow becomes chaotic.

Keywords: unsteady lid–driven square cavity flows, chaos, time series analysis, third Hopf bifurcation

PACS: 05.45.Pq, 05.70.Jk **DOI:** 10.1088/1674-1056/ac3226

1. Introduction

In the past 60 years, research into two-dimensional (2D) flows in a lid–driven square cavity has been regarded as a benchmark study.[1–6] The shape of this model makes it relatively simple to validate the accuracy and reliability of new methods by comparison with the benchmark solution.

In recent decades, researchers have shifted research focus to studying the Hopf bifurcations. The early studies on Hopf bifurcation mainly focused on the first bifurcation, in which the flow transfers its stationary state to a non-stationary periodic state. In a former work,[3] it was suggested that the first Hopf bifurcation occurs when the critical Reynolds number of Re_{c1} is larger than 7500. Since then various results have been given. It has been given as about $Re_{c1} = 7763 \pm 2\%$,[7] close to $Re_{c1} = 8000$[8] or greater than 8000, or about $Re_{c1} \in (8000, 8050)$,[9] while some authors localized in the interval of $(10000, 10500)$.[10] All the above work adopted a numerical simulation method. In theoretical analysis, Fortin *et al.*[11] predicted the critical Reynolds number of $Re_{c1} = 8000$ for the first Hopf bifurcation, through an eigenvalue analysis of the linearized Navier–Stokes equations. Thus, both theoretical analysis and numerical simulation disclosed that the critical Reynolds number for occurrence of the first bifurcation is located in the interval of $(7500, 10500)$. With increasing Reynolds number, the flow experiences a transition from the first Hopf bifurcation to the second Hopf bifurcation, in which the flow transfers its non-stationary periodic state to a quasi-periodic state. To date, one can only use numerical simulations to make these investigations and very few results have been disclosed for the second Hopf bifurcation. Auteri *et al.*[12] numerically forecasted the second Hopf bifurcation with a critical Reynolds number Re_{c2} located in the interval of $(9685, 9765)$. Wang *et al.*[13] numerically identified the critical Reynolds number of the second Hopf bifurcation to be located in the interval of $(11093.75, 11094.3604)$. They also discovered that there are two dominant frequencies and the phase diagram changes from an ellipse closed form to a non-ellipse closed form when the flow experiences a transition from the first Hopf bifurcation to the second Hopf bifurcation.

As the Reynolds number further increases, we expect the flow to experience a transition from the second Hopf bifurcation to the third Hopf bifurcation, in which the flow transfers its quasi-periodic state to a chaotic state. To date, there are no studies on the third Hopf bifurcation.

In this work, we apply the consistent fourth-order compact finite difference scheme[15] to study the third Hopf bifurcation and beyond in the lid–driven square cavity. We compute the critical interval of the third Hopf bifurcation and analyze the chaotic properties by Fourier analysis. We discover that the flow becomes chaotic beyond the third Hopf transition with a type of period-doubling feature. Further analysis of the phase diagram, Kolmogorov entropy and maximal Lyapunov exponent confirms our findings.

*Project supported by the National Natural Science Foundation of China (Grant No. 12162001), the Natural Science Foundation of Ningxia (Grant No. 2019AAC03129), and the Construction Project of First-Class Disciplines in Ningxia Higher Education (Grant No. NXYLXK2017B09).

†Corresponding author. E-mail: liutg@buaa.edu.cn

© 2021 Chinese Physical Society and IOP Publishing Ltd

2. Model description and numerical method

2.1. Governing equations

In this paper, two-dimensional lid–driven square cavity problems are considered and governed with the two-dimensional incompressible Navier–Stokes equations given in the non-dimensional vorticity–stream function form as

$$\psi_{xx}+\psi_{yy}=-\xi, \tag{1}$$

$$\xi_t+u\xi_x+v\xi_y=\frac{1}{Re}(\xi_{xx}+\xi_{yy}), \tag{2}$$

where u and v are the velocity components in the x- and y-directions respectively, Re is the Reynolds number, ψ is the stream function and ξ is the vorticity function, and $u=\psi_y$, $v=-\psi_x$. Equation (1) is referred to as the stream function equation, equation (2) is referred to as the vorticity equation.

The non-dimensional computational domain is set to $\{(x,y)|:0\le x\le 1,0\le y\le 1\}$. The boundary conditions are given as follows:

$$\begin{cases} y=1: & u=1,\ v=0,\ \psi=0,\\ y=0: & u=0,\ v=0,\ \psi=0,\\ x=0,1: & u=0,\ v=0,\ \psi=0. \end{cases}$$

Because the vorticity on the wall is unknown, in the process of solving Eq. (2), the condition of vorticity on the boundary must be supplemented. In this paper, the numerical boundary conditions of vorticity in Ref. [14] are used, namely,

$$\begin{aligned} &h(6\xi_1+4\xi_2-\xi_3)/21+O(h^4)\\ &=(15\psi_1-16\psi_2+\psi_3)/(14h)\pm V_{\rm w}. \end{aligned}$$

Here, the subscripts 1, 2, 3 represent the boundary point, its neighbor and its sub-neighbor points respectively. $V_{\rm m}$ is the tangential velocity of the wall. On the sliding wall, $V_{\rm w}=1$. On the solid wall, $V_{\rm w}=0$.

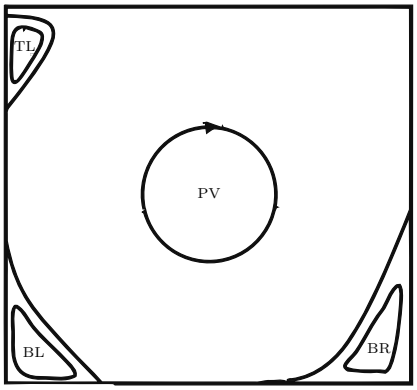


Fig. 1. Schematic of lid–driven square cavity.

At first, an unexpected balance of viscous and pressure forces causes the fluid to turn into the unit square cavity. The properties of these forces depend upon the Reynolds number, and a hierarchy of eddies develops. First, a larger clockwise-rotating primary vortex (PV) arises. Its location occurs toward the geometric center of the unit square cavity. Then, several small eddies arise: counterclockwise-rotating secondary eddies, and clockwise-rotating tertiary eddies. Their locations occur at the three relevant corners of the square cavity (bottom right (BR), bottom left (BL), and top left (TL)), appearing hierarchically at the inclined ellipses in Fig. 1.

2.2. Numerical method

As the Reynolds number increases, the flow instability starts from the wall boundary layer, where it becomes much thinner under a high Reynolds number. Thus, to predict the third Hopf bifurcation, the boundary layer has to be resolved accurately with either a very fine mesh or high-order numerical method. This makes the numerical simulation very costly and challenging. Eeven worse, recently, it has been found by us[15] that a high-order method might suffer from numerical instability inside the wall boundary layer if a lower-order treatment of boundary conditions is equipped. Such lower-order techniques of wall treatment are very popular in applications of high-order numerical methods. To fix this problem, we have developed a consistent fourth-order compact finite difference scheme,[15] in which both the order of accuracy and the major truncation error term are kept the same for the inner and boundary schemes. Such a high-order scheme can efficiently suppress the numerical instability inside the wall boundary layer. In this work, the numerical method employed is the consistent fourth-order compact finite difference scheme.[15]

After spatial discretization with the consistent fourth-order compact finite difference scheme, an explicit third-order TVD Runge–Kutta scheme[16] is used to perform time discretization.

Mesh convergency for the numerical method is carried out with a driven square cavity with $Re=12500$. Table 1 shows the values of velocity at a fixed point $(x,y)=(0.5,0.5)$ of the cavity when the fluid reaches the quasi-periodic state ($t=3000$) using three uniform meshes (65×65, 129×129, and 257×257) at $Re=12500$. It can be seen that the results under grid 129×129 are in good agreement with those under the fine grid 257×257 and the maximum error is less than 0.1%.

Table 1. Comparison of the values of velocity at a fixed point $(x,y)=(0.5,0.5)$ of the cavity when the fluid reaches the quasi-periodic state at $Re=12500$.

Grid points	u-velocity value	Error	v-velocity value	Error
65×65	−0.024567	3.002%	0.009712	2.391%
129×129	−0.023851	0.008%	0.009950	0.030%
257×257	−0.023853	–	0.009953	–

Based on the mesh convergence test of the above benchmark simulation, in this paper, we take a time step size of $\Delta t=1\times10^{-3}$ and solve the system with 129×129 uniform grids in the numerical simulations.

3. Third Hopf bifurcation

3.1. Scenario for the transition to chaos

We determine the different states of the flow according to the time evolution of velocity at a fixed point $(x,y) = (0.5,0.5)$ of the cavity. It is well known that the flow in a lid–driven square cavity becomes quasi-periodic when the Reynolds number is larger than a critical number of Re_{c2}, which is beyond 10000. The flow at $Re = 12500$ is still quasi-periodic in its second Hopf bifurcation as disclosed by Wang *et al.*[13]

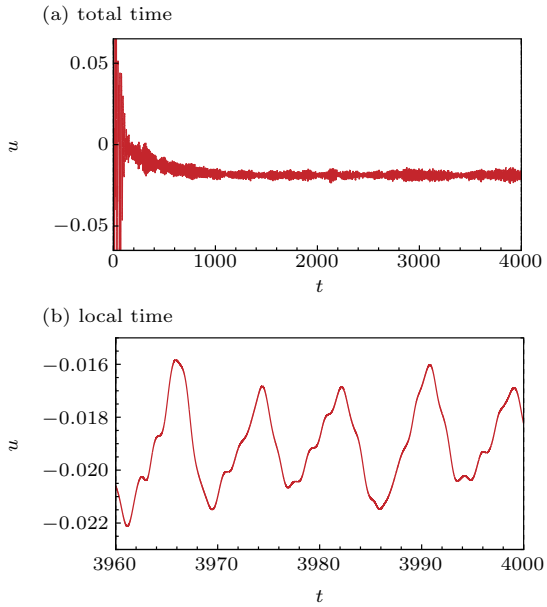


Fig. 2. Time history of u-velocity for $Re = 20000$.

We first calculated the flow with a higher $Re = 20000$ for t from 0 to 4000 as shown in Figs. 2(a) and 3(a) for the evolution of u-velocity and v-velocity at the geometric center point.

We enlarged Figs. 2(a) and 3(a) for t from 3960 to 4000 and found that the flow was under chaos as shown in Figs. 2(b) and 3(b) for evolution of the respective u- and v-velocity components at the geometric center point. From the enlarged figures, one can observe that the flow eventually evolves into a chaotic state.

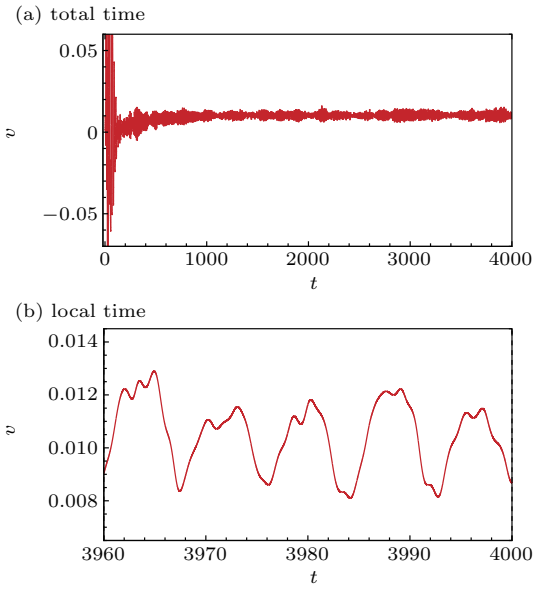


Fig. 3. Time history of v-velocity for $Re = 20000$.

3.2. Critical Reynolds number of the third Hopf bifurcation

The above results at $Re = 12500$ and $Re = 20000$ imply that the critical Reynolds number of Re_{c3} is located between 12500 and 20000. We began to find Re_{c3} by the method of bisection. Starting from $a_0 = 12500$, $b_0 = 20000$, if at $Re = (a_k + b_k)/2$, we get quasi–periodic solution, then we let $a_k = (a_k + b_k)/2$; If at $Re = (a_k + b_k)/2$ we get a chaos solution, then we let $b_k = (a_k + b_k)/2$. We repeated this process and carried out the dichotomy for 12 times, and we got a very small interval. Finally, in this way, Re_{c3} was localized in the small interval $(13944.7021, 13946.5333)$. Table 2 shows the process of localizing the range of Re_{c3} by bisection.

In a series of Figs. 4 and 5, we present the time history of $u(t)$ for different Reynolds numbers. In these graphs, we can clearly see that during the process of determining the critical Reynolds number, the function $u(t)$ solution is either quasi-periodic or chaotic.

Table 2. Process of bisection for confirming Re_{c3}.

k	a_k	b_k	$(a_k + b_k)/2$	Solution	Re_{c3}
0	12500	20000	16250	chaotic	(12500, 16250)
1	12500	16250	14375	chaotic	(12500, 14375)
2	12500	14375	13437.5000	quasi–periodic	(13437.5000, 14375)
3	13437.5000	14375	13906.2500	quasi-periodic	(13906.2500, 14375)
4	13906.2500	14375	14140.6250	chaotic	(13906.2500, 14140.6250)
5	13906.2500	14140.6250	14023.4375	chaotic	(13906.2500, 14023.4375)
6	13906.2500	14023.4375	13964.8438	chaotic	(13906.2500, 13964.8438)
7	13906.2500	13964.8438	13935.5469	quasi-periodic	(13935.5469, 13964.8438)
8	13935.5469	13964.8438	13950.1954	chaotic	(13935.5469, 13950.1954)
9	13935.5469	13950.1954	13942.8712	quasi-periodic	(13942.8712, 13950.1954)
10	13942.8712	13950.1954	13946.5333	chaotic	(13942.8712, 13946.5333)
11	13942.8712	13946.5333	13944.7021	quasi-periodic	(13944.7021, 13946.5333)

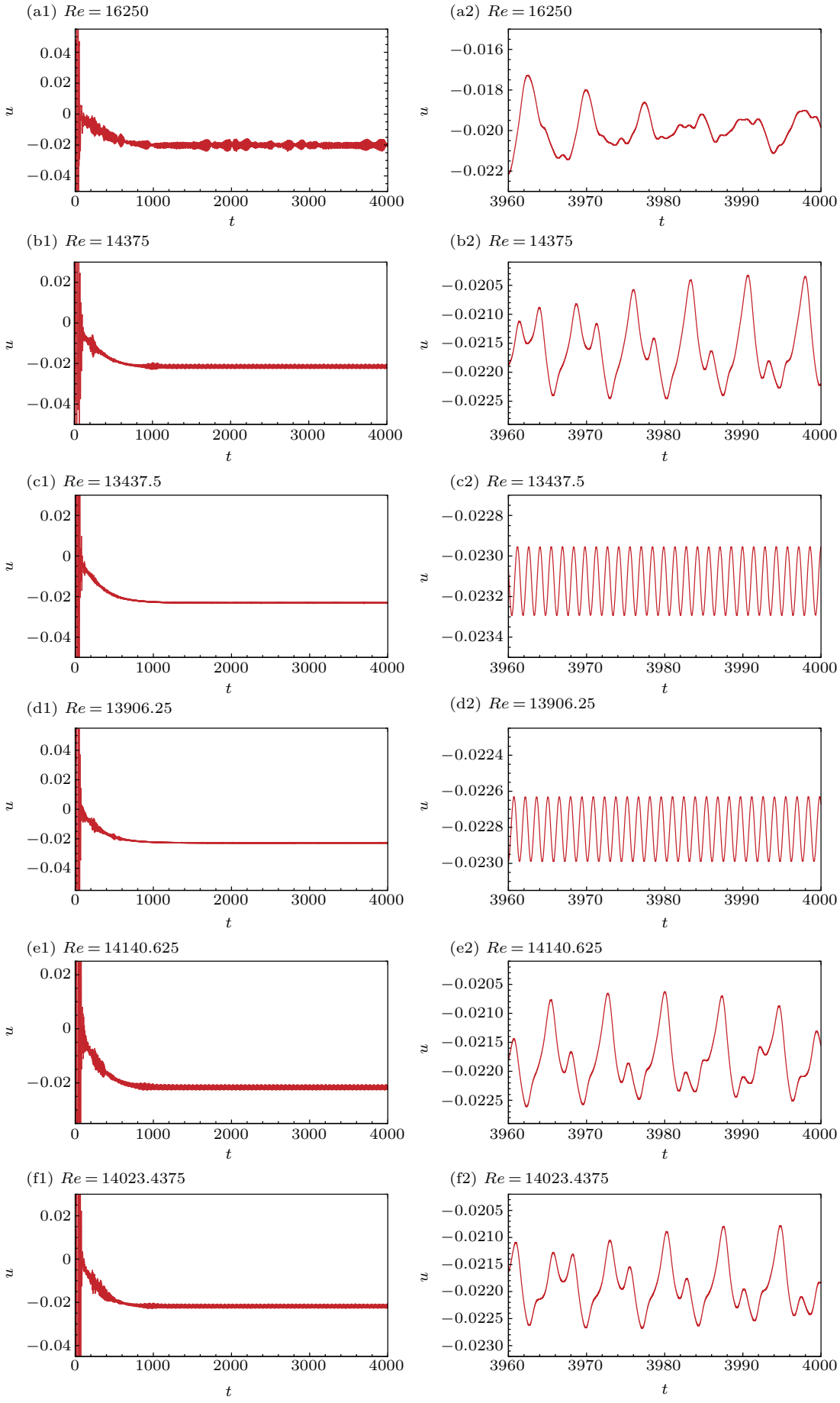


Fig. 4. Time history of u-velocity for different Reynolds numbers: (1) total time; (2) local time.

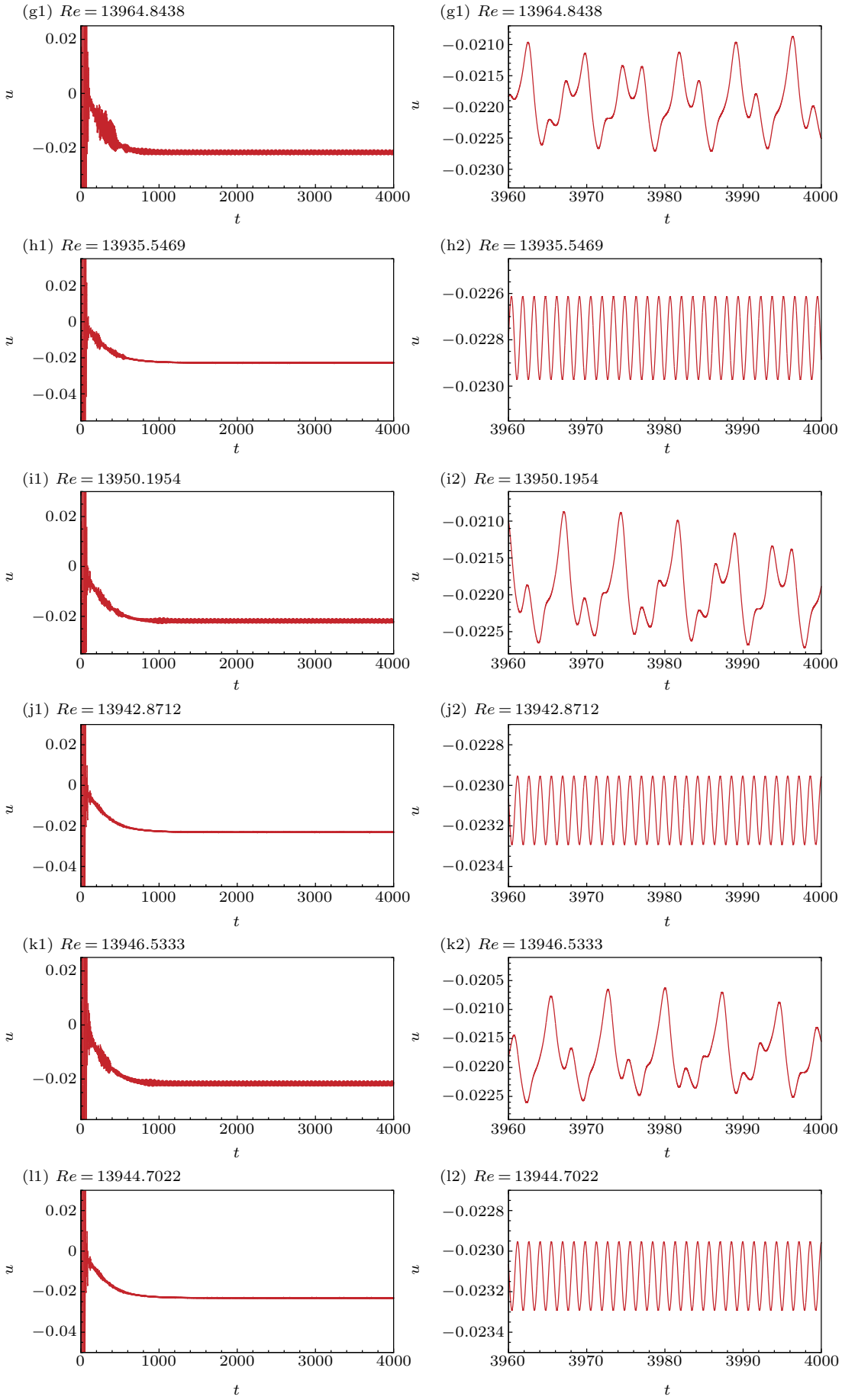


Fig. 5. Time history of u-velocity for different Reynolds numbers: (1) total time; (2) local time.

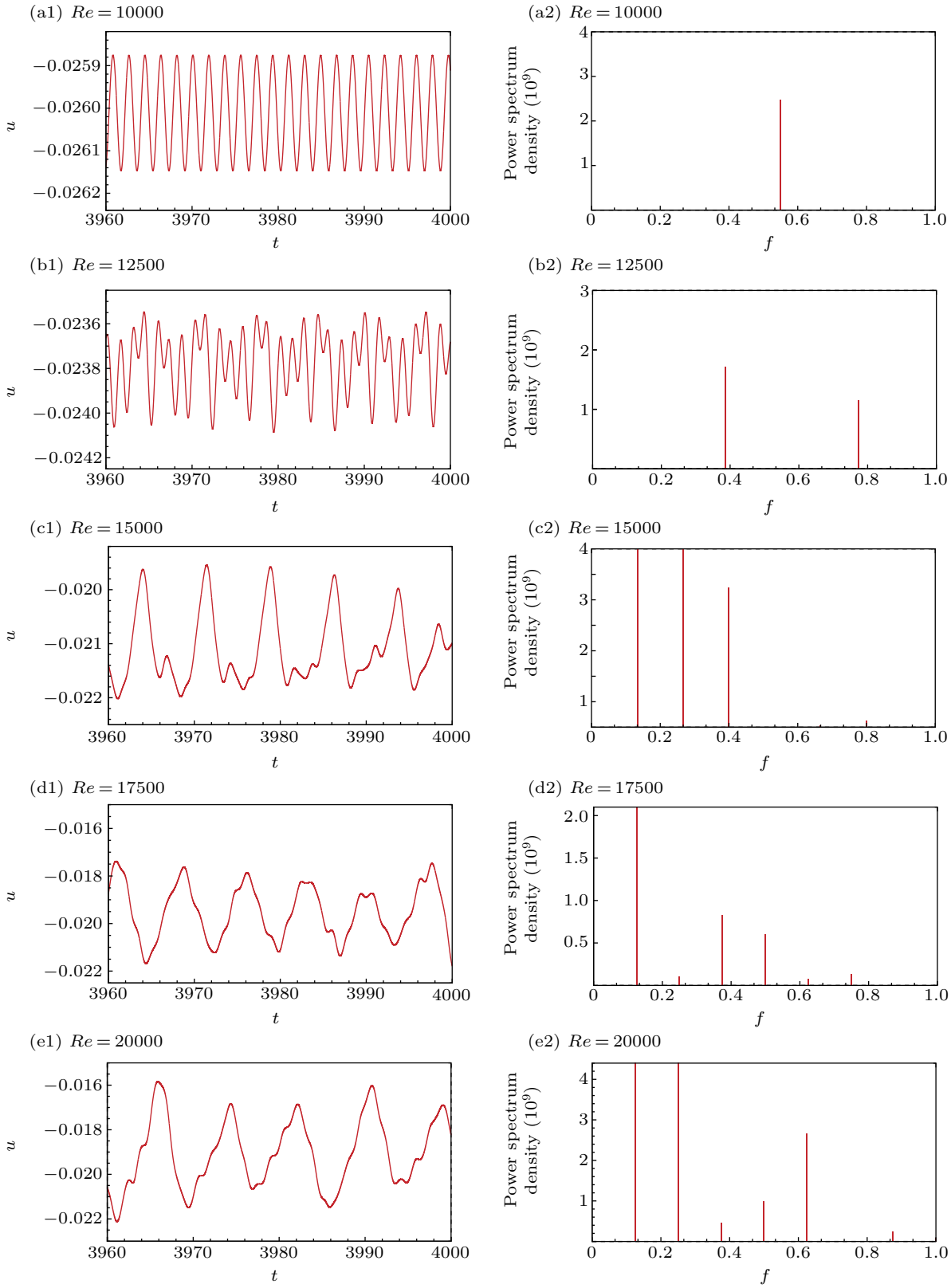


Fig. 6. (a1)–(e1) Time history (left figures) of u-velocity from $t = 3960.0$ to $t = 4000.0$; (a2)–(e2) power spectrum density (right figures) of u-velocity for different Reynolds numbers.

3.3. Type of third Hopf bifurcation

The nontrivial succession of periodic, quasi-periodic and eventually seemingly random regimes is reminiscent of the transition to chaos.

It can be seen from Ref. [17] that the route of chaos follows one of the three canonical scenarios: the Ruelle–Takens–Newhouse scenario;[18] the Feigenbaum scenario;[19,20] or the Pomeau–Manneville scenario.[21] The characteristic features of each of these scenarios can be tracked from the evolution of

the dominating frequencies of the system.[22] Thus, we shall analyze the main frequencies of velocity fluctuations and seek which classical scenario follows during the flow transition to chaos in the cavity.

We focus on the evolution of $u(t)$ for different Reynolds numbers from $t = 3960$ to $t = 4000$ as shown in Figs. 6(a1)–(e1). Without loss of generality, we analyze the time series data of u in Figs. 6(a2)–(e2) via the power spectrum density (PSD). The PSD $s(\omega)$ is the square mean of the Fourier transform $F_(t)$ of the sample time series,

$$S(\omega) = \frac{1}{T}|F_t(\omega)|^2 = \frac{1}{T}(A^2 + B^2), \tag{3}$$

where A and B are the real and imaginary parts of the complex number, respectively. We use f to express the frequency and $f = 1/T$. The time series and power spectrum of velocity u are given in Figs. 6(a2)–6(e2). In these figures, the left figures shows the time series of u at different Reynolds numbers, and their corresponding PSDs are shown in the right figures. At $Re = 10000$ as shown in Fig. 6(a2), there is only a frequency indicating the flow is periodic. When the Reynolds number increases, we can see that the flow tends to be quasi-periodic with two frequencies at $Re = 12500$. The flow becomes chaotic with four frequencies as Re increases to $Re = 15000$ from Fig. 6(c2). The number of frequencies increases to six when $Re = 17500$ as observed in Fig. 6(d2). Further, as Re increases to $Re = 20000$, the number of frequences increases to eight with two primary frequencies and six secondary frequencies found from Fig. 6(e2). The series of PSD figures shows no existence of odd number frequencies and exhibits a characteristic of period-doubling bifurcation.

4. Characterization of the dynamical system

Theoretically, a chaotic dynamical system cannot be fully characterized by means of frequency spectra. In particular, spectra do not offer a way to distinguish a stochastic system from a chaotic one. To ascertain the possible chaotic nature of the flow system in the cavity, most scholars seek to characterize the underlying dynamics by means of nonlinear time series analyses of the attractor,[23] Kolmogorov entropy[24] and maximal Lyapunov exponent.[25,26] In this paper,we also ascertain it by these means.

4.1. Attractor

We reconstruct the two-dimensional phase space of the time series of $u(t)$ from $t = 3960$ to $t = 3964$ at different Reynolds numbers.

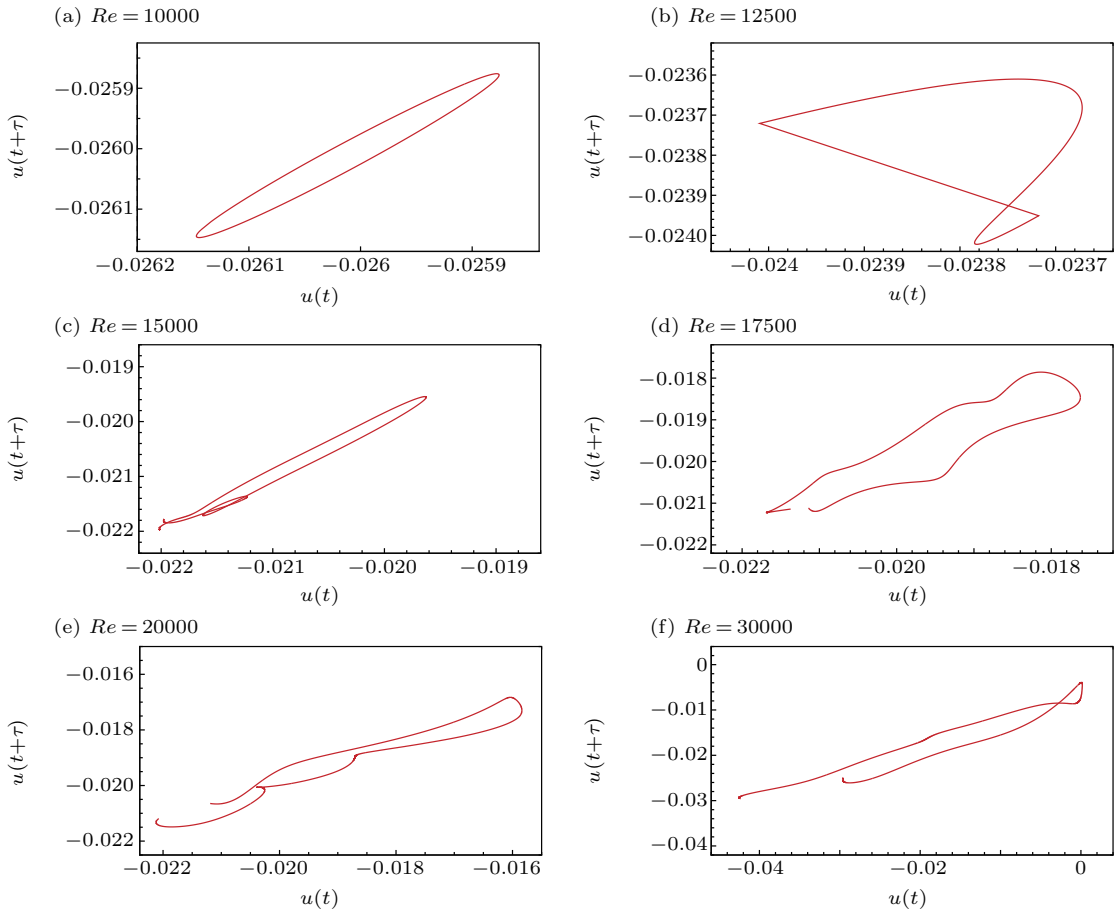


Fig. 7. Phase portrait of $u(t)$ for different Reynolds numbers.

Packard[27] proposed to reconstruct the phase space equivalent to the original phase space of the system by restoring the attractor of the dynamical system from scalar time series. The time delay method is to reconstruct the phase space by selecting the appropriate time delay and embedding dimension for the one-dimensional time series and further observe the attractor characteristics of the phase space. According to embedding theory,[28] it can be reconstructed by selecting the appropriate reconstruction dimension m and delay time τ for the one-dimensional time series and an m-dimensional phase space can be reconstructed. In this paper, we rearrange the original time series into a two-dimensional distribution ($m = 2$), namely,

$$U = [U_1, U_2] = \begin{bmatrix} u_{t_1} & u_{t_1+\tau} \\ u_{t_2} & u_{t_2+\tau} \\ u_{t_3} & u_{t_3+\tau} \\ \vdots & \vdots \\ u_{t_n} & u_{t_n+\tau} \end{bmatrix}. \tag{4}$$

The autocorrelation method[29] is used to calculate the time delay τ. We calculate the time delay $\tau = 1.818, 1.429, 7.500, 7.500, 8.000, 9.2000$ for $Re = 10000, 12500, 15000, 17500, 20000, 30000$.

Then, we can draw a two-dimensional phase distribution to study the evolution of its phase diagram and attractor of the system with Eq. (4). Figures 7(a)–(f) show the evolution of the phase diagram and thus the characteristics of the attractor at various Reynolds numbers. The series of phase diagrams shows a change from an ellipse closed form at the periodic state to a non-ellipse closed form at the quasi-periodic state and finally to an unclosed curve. The attractor of the system changes from the normal to a strange one. This implies that the flow system eventually becomes chaotic when $Re \in [Re_{c3}, 30000]$.

4.2. Kolmogorov entropy

We compute the Kolmogorov entropy (denoted by K) of the time series of $u(t)$ from $t = 0$ to $t = 4000$ for different Reynolds numbers.

The Kolmogorov entropy can be computed by the method proposed in Ref. [30]. Theoretically, a chaotic (deterministic) system is characterized with a positive finite value of $0 < K < \infty$; an order system has a value of $K = 0$, and a random system holds a value of $K = \infty$.

At present, the correlation integral $C_2(m, \varepsilon)$ is widely used in the literature to calculate K, called the correlation entropy. The specific calculation process is as follows: (i) For the time series $u(t)$, we reconstruct the phase space $U(t)$ according to form Eq. (4); two of the vectors are U_i (i.e. $i = 1, 2$). (ii) The Euclidean distance from the remaining $n-1$ points to U_i is calculated by selecting any point from the n points in U_i

$$r_{ij} = d(U_i - U_j) = \left[\sum_{l=1}^{m} (u_{i+l\tau} - u_{j+l\tau}) \right]^{\frac{1}{2}}. \tag{5}$$

(iii) Given a critical distance of r, the proportion of the logarithm of points whose distance is less than r over all points is the correlation integral $C_m(r)$, then,

$$C_m(r) = \frac{1}{n^2} \sum_{i \neq j} H\left(r - |U_i - U_j|\right). \tag{6}$$

(iv) Repeat this process to exhaust all phase points to obtain the associated integral function K_2, calculated by the following formula:

$$K_{2,m}(r) = \frac{1}{\Delta m} \ln \frac{C_m(r)}{C_{m+\Delta m}(r)}, \tag{7}$$

$$K_2 = \lim_{\substack{r \to 0 \\ m \to \infty}} K_{2,m}(r), \tag{8}$$

K_2 entropy is usually used as an approximation of K.

Table 3 shows the value of K is zero for Re equal to 10000 or 12500. Thus the system is in order. This is consistent with the conclusion of Ref. [13]. The value of K is greater than zero for $15000 \leq Re \leq 20000$. Thus the system is in chaos. We continue to calculate the K value for $Re = 25000, 30000$; the value of K increases with increasing Reynolds number. As a result, the flow system in the cavity is chaotic for $Re \in [Re_{c3}, 30000]$.

Table 3. Kolmogorov entropy for different Reynolds numbers.

Re	10000	12500	15000	17500	20000	25000	30000
K	0	0	3.7820	4.3366	4.6336	4.7254	6.3224

Figure 8 shows the variation of the K value for different Reynolds numbers. It shows that as Re increases, the value of K increases.

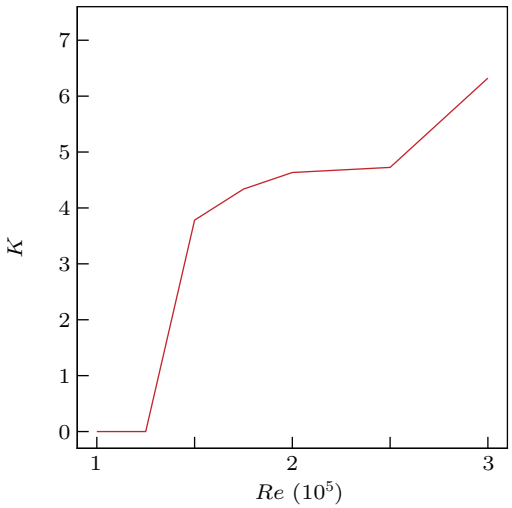


Fig. 8. Variation of K value for different Reynolds numbers.

In order to observe the subtle changes of the whole flow field more clearly, without loss of generality, we give the two-dimensional stream function contours for different Reynolds

numbers. Figure 9 shows the contours of the stream function for $Re = 20000, 30000$. It can be seen from Fig. 9 that the streamlines in the middle of the cavity are smooth while in three corners of the cavity they are twisted. This is why the values of K are not as large.

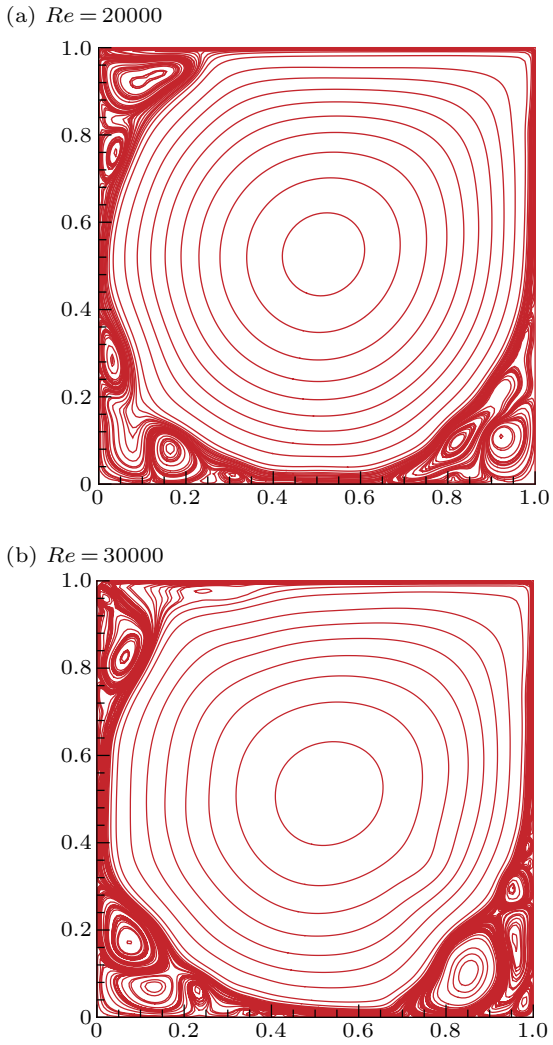


Fig. 9. Streamlines for different Reynolds numbers.

4.3. Maximal Lyapunov exponent

The chaotic behavior at $Re \in [Re_{c3}, 30000]$ can be characterized further by computing the maximal Lyapunov exponent (denoted by λ). λ is computed as the rate of spatial divergence in the phase space of two trajectories that are initially in the same neighborhood.[31] In a deterministic system, the existence of dynamic chaos can be intuitively judged from whether the maximum Lyapunov exponent is greater than zero. If the maximum Lyapunov exponent of the system is positive ($\lambda > 0$), the system is chaotic; the higher the value is, the more chaotic the system is. Otherwise, the system is ordered ($\lambda \leq 0$).

Here, we apply the Wolf method[32] to compute λ of the time series of $u(t)$ from $t = 0.0$ to $t = 4000.0$ for different Reynolds numbers. The specific calculation process is as follows: For the time series $u(t)$, we (i)reconstruct the phase space $U(t)$ according to form Eq. (4), (ii) take the initial point $U_0(t_0)$ and find the nearest neighbor of the initial point $U_0(t_0)$, let it be $U(t_0)$ and then let the Euclidean distance between the two points be L_0, (iii) track the evolution trajectory of $U_0(t_0)$ and $U(t_0)$ with time until t_1, when the distance between them exceeds a certain specified value $\varepsilon > 0$: if $L_0' = |U(t_1) - U_0(t_1)| > \varepsilon$ then keep $U(t_1)$ and find another point $U_1(t_1)$, such that $L_1 = |U(t_1) - U_1(t_1)| < \varepsilon$ and the angle between them is as small as possible, (iv) continue the above process until $U(t)$ reaches the end point N (N is the length of the time series). Let the total number of iterations in the evolution process be M; then the formula for λ is

$$\lambda = \frac{1}{t_m - t_0} \sum_{i=0}^{M} \ln \frac{L_i'}{L_i}. \tag{9}$$

We obtain λ for different Reynolds numbers. The results are shown in Table 4. Table 4 shows the value of λ is 0 for Re equals to 10000 or 12500. Thus the system is in order. This is again consistent with the conclusion of Ref. [13]. The value of λ is greater than 0 for $15000 \leq Re \leq 20000$, which confirms the chaotic behavior of the system. We continue calculate the λ value for $Re = 25000, 30000$ and find $\lambda > 0$. As shown in Fig. 10, one can see the variation of λ value for different Reynolds numbers. The value of λ increases as Re increases.

In conclusion, the various nonlinear analyses above confirm the presence of chaos for $Re \in [Re_{c3}, 30000]$.

Table 4. Maximal Lyapunov exponent for different Reynolds numbers.

Re	10000	12500	15000	17500	20000	25000	30000
λ	0	0	0.6203	1.0745	2.2534	2.3043	4.1759

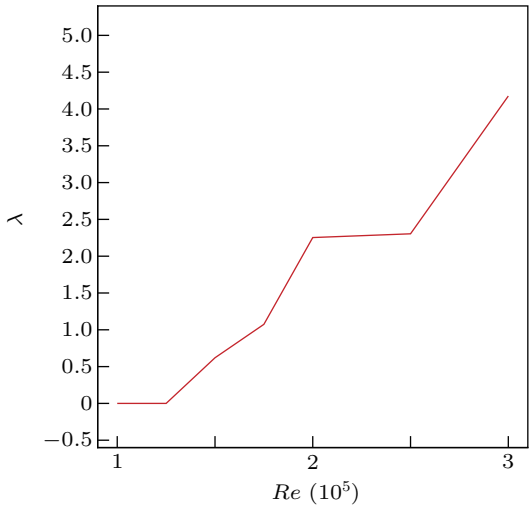


Fig. 10. Variation of λ value for different Reynolds numbers.

5. Conclusion

In this paper, we presented a numerical investigation on the pathway to chaos in driven square cavity flow.The flow

dynamics were analyzed by means of the time series of the u-velocity component obtained by direct numerical simulation of the unsteady two-dimensional Navier–Stokes equations. As a first result, we confirmed the existence of the third Hopf bifurcation as the Reynolds number increases and located the critical Reynolds number of the third Hopf bifurcation (Re_{c3}) in the interval of (13944.7021,13946.5333).

Moreover, by analyzing the time series of the u-velocity component, we disclosed that its successive bifurcation is period-doubling and the flow becomes chaotic when the Reynolds number is beyond Re_{c3}. The chaotic characteristics were further confirmed via analysis of the Kolmogorov entropy, maximum Lyapunov exponent and phase diagram.

Acknowledgment

The authors thank Professor Yong Xu of the Northwestern Polytechnical University for helpful discussion.

References

[1] Ghia U, Ghia K and Shin C T 1982 *J. Comput. Phys.* **48** 387
[2] Orlandi O 1987 *Comput. Fluids* **15** 137
[3] Hou S, Zou Q, Chen S, Doonlen G and Cogely A 1995 *J. Comput. Phys.* **118** 329
[4] Erturk E 2006 *Int. J. Numer. Meth. Fluids* **50** 421
[5] Erturk E 2009 *Int. J. Numer. Meth. Fluids* **60** 275
[6] Nuriev A N, Egorov A G and Zaitseva O N 2016 *Fluid Dyn. Res* **48** 61405
[7] Poliashenko M and Aidun C K 1995 *J. Comput. Phys.* **121** 246
[8] Boppana V B L and Gajjar J S B 2010 *Int. J. Numer. Meth. Fluids* **62** 827
[9] Bruneau C H and Saad M 2006 *Comput. Fluids* **35** 326
[10] Shen J 1991 *J. Comput. Phys.* **95** 228
[11] Fortin A, Jardak M, Gervais J and Pierre R 1997 *Int. J. Numer. Meth. Fluids* **24** 1185
[12] Auteri F, Parolini N and Quartapelle L 2002 *J. Comput. Phys.* **183** 1
[13] Wang T, Liu T G and Wang Z 2020 *Chin. Phys. B* **29** 030503
[14] Gupta M M 1998 *Int. J. Numer. Meth. Fluids* **28** 737
[15] Wang T and Liu T G 2019 *Numer. Math.: Theory, Methods and Applications* **12** 312
[16] Shu C W and Osher S 1988 *J. Comput. Phys.* **77** 439
[17] Launay G, Cambonie T, Henry D, Pothérat A and Botton V 1988 *Phys. Rev. Fluids* **4** 044401
[18] Newhouse S, Ruelle D and Takens F 1978 *Comm. Math. Phys.* **64** 35
[19] Feigenbaum M J 1979 *Phys. Lett. A* **74** 375
[20] Feigenbaum M J 1980 *Comm. Math. Phys.* **77** 65
[21] Pomeau Y and Manneville P 1980 *Comm. Math. Phys.* **74** 189
[22] McCauley J L 1994 *Chaos, Dynamics and Fractals: An Algorithmic Approach to Deterministic Chaos* (1st edn.) (Cambridge: Cambridge University Press) pp. 1–22
[23] Ding P F, Feng X Y and Wu C M 2020 *Chin. Phys. B* **29** 108202
[24] Verstappen R, Wissink J G and Veldman A E P 1993 *Appl. Sci. Res.* **51** 377
[25] Gao F, Hu D N and Tong H Q 2018 *Acta Phys. Sin.* **67** 150501 (in Chinese)
[26] Zhang L P, Liu Y and Wei Z C 2020 *Chin. Phys. B* **29** 060501
[27] Packard N H 1980 *Phys. Lett. A* **45** 712
[28] Takens F 1981 *Lect. Notes Math.* **898** 366
[29] Abarbanel H D I, Brown R, Sidorowich J J and Tsimring L S 1993 *Rev. Mod. Phys.* **65** 1331
[30] Grassberger P and Procaccia I 1983 *Phys. Rev. A* **28** 2591
[31] Rosenstein M T, Collins J J and De Luca C J 1993 *Physica D* **65** 117
[32] Wolf A, Swift J, Harry Swinney L and Vastano J 1985 *Physica D* **16** 285